

# Analytical and Experimental Research for Development of the Airless Tires for Urban Micromobility Means

ALEXANDER VOLOCHKO

SSI "Physical-Technical Institute of the National Academy of Sciences of Belarus"

10, Kuprevich str., Minsk, 220084

REPUBLIC of BELARUS

STSIAPAN YANKEVICH

OJSC "Instrument Making Plant Optron"

52, F.Skoriny str., Minsk, 220084

REPUBLIC of BELARUS

NATALLIA YANKEVICH

SSI "Center for the System Analysis and Strategic Research of the National Academy of Sciences of Belarus"

1, Academicheskaya str., Minsk, 220072

REPUBLIC of BELARUS

*Abstract:* It is currently recognized that electric vehicles are the optimal type of passenger transport for urban usage. However, there are very few people willing to buy them, since today electric cars are very expensive. So the development of the personal light electric transport segment (electric bicycles, scooters, motorcycles, etc.) becomes very relevant. At the same time, the introduction of new technologies (in particular, 3D printing) and constructions (airless wheels) for their mass production is of particular importance.

The range of problems that can be solved by modern additive technologies is expanding every day. FDM technology is one of the most commonly used additive methods. It is not only widely available, but it also provides significant possibilities for decision-making. However, most developments in this area are focused on obtaining the geometric accuracy of shapes without taking into account the mechanical properties of materials used. Therefore, the purpose of this study is to investigate experimentally the influence of filling density of parts manufactured by 3D printing on their mechanical properties and application of obtained results for the production of airless tires by using FDM technology.

*Key-Words:* Mathematical modeling, 3D printing, additive technologies, airless tires

Received: July 27, 2023. Revised: February 11, 2024. Accepted: March 15, 2024. Published: May 16, 2024.

## 1 Introduction

The opportunities provided by additive technologies can be effectively used in the production of a wide range of parts. However, this requires carrying out a complex of works not only in the field of design development as such, but also in justifying the choice of materials and technologies used.

For example, there exists a considerable interest in the production, in particular, of airless wheels that combine the functions of a wheel and a shock absorber in their design. In addition, usage of airless tires allows not only to eliminate completely the loss

of vehicle mobility, but also to obtain solutions that can be widely used in the operation of autonomous automatic vehicles.

As it is known, a conventional tire, consisting mainly of a reinforced toroid mounted on a metal rim, is the product of complex composites. Since the appearing of the non-pneumatic tires (airless wheels), the most common concept has been to use a layer of elastomer with reinforced rings and a distinctive spoke structure attached to the inside part of the tire and evenly distributed around the rim.

Currently, one of the most common solutions for airless wheels is to replace the air within the toroidal

volume around the rim with discrete spokes distributed evenly between the inner and outer rings. The spokes in such structures play the role of elastic elements that deform or bend in accordance with the magnitude of the load applied in the radial direction and, therefore, provide the necessary rigidity.

The complexity of the design of airless wheels requires introduction of new technologies (in particular, additive manufacturing methods), as well as improvement of both computational and experimental research methods that would take into account as much as possible the properties of the materials used, the mutual influence of structural elements and loading conditions.

The developed approaches are universal in nature and can be used for solution a number of practical problems.

## 2 Problem Formulation

According to statistics in the world, 90% of drivers drive no more than 90 km daily. This makes it urgent to develop the segment of personal electric transport (electric scooters, electric bicycles, electric motorcycles, electric scooters, unicycles, hoverboards, etc.), which are an excellent alternative to a car. The trend towards increasing popularity of personal electric transport in the world has been evident several years ago. For several years now, experts in the United States and European countries have noted the spread of ideas of abandoning the car in favor of bicycles, scooters and electric vehicles. In addition, the spread of home delivery of food and groceries is having a strong impact (couriers and delivery people are increasingly choosing electric vehicles as a more efficient alternative to conventional bicycles and cars). The appearance on the market of a large number of high-quality and, most importantly, inexpensive models of electric bicycles and electric scooters also stimulates the development of this particular segment of electric transport [1, 2].

At the same time, namely the market of light electric scooters showed the most active rate of growth in popularity (according to various sources, the demand for light electric scooters in 2020 increased, despite the COVID-19 epidemic, by an average of 1.5–1.6 times compared to the previous year). If in 2017 the global electric scooter market was valued at \$630 million (it accounted for 8% of the entire two-wheeled electric transport market excluding electric motorcycles), then according to expert forecasts, the share of light electric scooters will grow by 2024 to 14.5%.

There are several reasons for the growing popularity of light electric scooters:

- Mobility. The electric version of the scooter differs little from the regular one (slightly larger in size and weight).
- Power. Light electric scooters can reach speeds of up to 40-50 km/h.
- Road conditions and quality of public transport.
- Ecology. Conditions are being created for the growth of electric transport in developed countries: cars, scooters, light scooters.
- Improving the quality and operating time, reducing the cost of electric vehicles.
- Development and widening of sharing services.

At the same time, the introduction of new technological solutions that increase the competitiveness of developments in the field of personal light electric transport on the world market is relevant. Recently, this problem has become increasingly important due to the need to reduce intensively the specific weight of light electric scooters while simultaneously to increase their service life and reliability during operation. All this requires not only the introduction of new technologies, in particular, additive manufacturing methods, but also the improvement of both computational and experimental methods for studying promising designs as a whole as well as the constructions of their parts.

The range of problems that can be solved using modern additive technologies is expanding more and more every day. Problems appearing during the creation of conceptual samples as well as the production of the industrial products can be solved more easily with their help. Well-known attempts of manufacture experimental designs of electric motors, electric scooters, bicycles and motorcycles based on additive technologies, being implemented even at the level of experimental work, arouse significant interest in the scientific community and industrial organizations.

At the same time, usage of additive technologies requires a set of works in the development of the design of components of personal electric vehicles, as well as in terms of justifying the choice of materials and technologies used. 3D printing technology, while relatively widely available, provides researchers and manufacturers with significant decision-making flexibility. Therefore, resolving issues related to the technological aspects of this method (filling density of the part, relative arrangement of layers, etc.) in order to improve the performance characteristics of manufactured structures still remain unresolved and require further research.

The opportunities provided by additive technologies can be effectively used in the production of airless

wheels, combining in their design the functions of a wheel and a shock absorber, which allows almost completely eliminate the loss of mobility of a personal light electric vehicle.

In this connection must be mentioned, that the first versions of airless tires appeared at the beginning of the last century, and often the reason for such projects was a shortage of materials (designers tried to replace hard-to-find and expensive rubber with more profitable wood or metal). Currently, the shortage problem has been resolved, and new projects are associated only with the desire to improve the performance of the chassis.

Early designs of airless tires often consisted of a metal disk and an outer rim with tread, connected by a set of springs of different shapes and configurations. Such designs generally solved the assigned problems, but turned out to be too complex and inconvenient to use.

Anyway, airless tires have not yet found widespread use due to their high rigidity and weak damping compared to conventional ones.

If airless tires are closed (with side walls), then it is difficult to distinguish them from ordinary pneumatic tires by their appearance.

Today there are two main designs in this area:

- tires filled with special fiberglass;
- tires, where the lack of air is compensated by the presence of polyurethane spokes [3].

The first ones are most often made closed so that the fiberglass does not get lost along the way. However, practice has shown more advantages of an open system: fewer materials, easier manufacturing, and any defects resulting from operation are much easier to notice. The design seems very simple: the edge of the tire is a tension clamp, the middle is a classic hub, to which polyurethane spokes are attached strictly in a certain sequence.

The basic design of airless tires, which is currently being actively developed, has both undeniable advantages and disadvantages that have not yet been corrected.

The main advantages of tires without air are:

- the ability to change shape depending on the bumps being driven;
- their service life without restoration is 2-3 times longer than analogues, 9 million of wheel's operation cycles;
- high performance (as long as at least 70% of its elements are present in the structure);
- there is no need to check the pressure, which means there is no need to carry additional tools (jack, pump, etc.);
- significantly less weight than classic tires. The complete absence of the need for disks (steel, cast,

forged, etc.) reduces the unsprung weight, which also leads to positive effects in driving;

- easy to operate, one-piece, monolithic and complete design;
- reducing the transported weight and, as a result, reducing fuel consumption;
- prices for airless tires (when they appear widely on the shelves) are unlikely to exceed pneumatic analogues;
- installation of airless tires will be available on absolutely any car in the future;
- significant comfort and safety for the operator, reduces fatigue and the risk of future occupational injuries for the operator.

The disadvantages include:

- the safe speed limit does not exceed 80 km/h before now;
- some designs also exhibit excessive noise and heating during prolonged high-speed operation;
- load capacity of such rubber (the technology is still imperfect);
- the rigidity of the structure is not adjustable in any way.

The emergence of airless automobile tires, whose performance indicators are not inferior to traditional pneumatic tires, is an important step towards increasing vehicle safety and the survivability of special automotive equipment. However, for a qualitative leap in the development of their design, a sufficient amount of scientific information has not yet been accumulated.

The first production samples of airless tires were developed for military purposes by the American company Resilient Technologies (2002). These developments were used on the Humvee military transport.

The Airless prototype (Resilient NPT) was developed in 2007 (it was tested in 2009). The tire was made of fire-resistant rubber and consisted of a frame made in the form of a "honeycomb" and a rubber rim with a tread. Such form factor makes it possible to achieve both sufficient rigidity (the wheel can hold heavy vehicles and perform its functions even when up to 30% of the cells are destroyed), and at the same time sufficient softness, because "honeycombs" are well deformed, overcoming road unevenness no worse than an air-filled tire.

The first "civilian" airless tires (named Tweel) were patented in 2005 by the French company Michelin. Tweel are used in various special equipment, scooters and wheelchairs, but their design had not been finalized yet for high speeds. Structurally, Tweel tire is a system of one-piece internal hubs attached to the axle shaft. Around them are

polyurethane knitting needles connected in a certain sequence. A tension collar runs through the spokes to form the outer edge of the tire. At the same time, Michelin managed to combine the rigidity necessary for reliability and softness, which civilian cars can't do without.

The Tweel design involves the usage of rubber spokes with a special cross-section (they act as air substitutes inside the tire). The purpose of rubber spokes is to eliminate impacts, which is realized even better than in the case of an inflated tire. The cross-section of the spokes is minimal, so it guarantees the stability of the tire even with severe deformations. As a result, the spokes bend only in one plane. Such tires are of the open type by their design. We should also highlight the lightness of the new product, the weight of which is less than that of a pneumatic wheel. With resistance to tearing and damage, long service life and ease of replacement, the prospect of switching to new tires becomes extremely tempting.

Michelin [4] has signed a contract to install new products on lunar rovers. Since 2012, these airless tires have been installed on construction equipment, loaders, and agricultural vehicles. The disadvantages of the design are the high price, insufficient load capacity, and the inability to change the level of rigidity (on a machine with conventional wheels, the pressure simply drops to the required level).

Polaris [5] became a competitor for Michelin. Structurally, these airless tires are quite similar, but Polaris replaced the spokes with a honeycomb system like a beehive. Composite materials were used in the development. The resulting cells, depending on the speed of movement, exhibit different rigidity parameters: sometimes they are rigid, sometimes they are flexible, and as a result, the shape of the wheel is better maintained when overcoming the irregularities.

Bridgestone airless tires feature spokes that twist in both directions in the profile, making the tire more resilient. In addition, Bridgestone proposed creating new tires from recycled old rubber. However, practice has shown the possibility of using such a design only in golf carts: the maximum speed is limited to 64 km/h, and the load capacity of one wheel is only 150 kg. In further research, Bridgestone engineers initially plan to consider such tires as a solution for commercial trucks, rather than passenger vehicles.

However, before Bridgestone introduces its airless tires to the truck market, it plans to release a lighter, smaller version for regular bicycles.

I-Flex airless tires (Hankook) were a breakthrough in the industry. The Korean company created tires [6] in which the tire and rim were one unit. In addition, I-Flex is made from 95% recycled materials. I-Flex tires, made in 14" size and having an original design, were shown for the first time at the Frankfurt Motor Show in 2013.

Developments in this field are actively underway, and serial copies have so far been used mainly on lightly loaded vehicles (lawn mowers, scooters, golf carts, etc.). Airless rubber is used in the industrial sector in excavators and loaders, and it is now sometimes used in personal transport in wheelchairs and bicycles. The reason for this selectivity is simple: the still imperfect design of the rubber at speeds above 80 km/h creates parasitic vibrations that are well transmitted to the car body.

However, Hankook successfully completed a series of tests on iFlex airless tires in 2015, during which the new tires proved that they are in no way inferior to conventional tires. In particular, the car with such tires accelerated to 130 km/h. Now similar airless tires are installed on Volkswagen Up.

Proving the perspectives of airless tire design is Goodyear's new Aero Concept, unveiled at the Geneva Motor Show (2019). This tire is designed for the movement of vehicles by air and on ordinary roads. Depending on the driving orientation, the Goodyear Aero concept operates differently. It has a multi-modal design that, when driven on the road, acts like a regular tire with spokes supporting the weight of the vehicle. To create vertical lift, the spokes are turned into propeller blades, like part of an airplane's propulsion system.

The new concept of tire's airless design makes it flexible enough to eliminate the shock of road driving, yet strong enough to spin at high speeds to create vertical lift.

It should be noted that both the above designs of airless tires and other developments of well-known companies (Uniroyal, Yokohama, Toyo, Boing, Ameritare, Sumitomo, etc.) have scientifically based technical solutions obtained as a result of theoretical research at the design stage. The development of such tires is now being carried out by recognized industry leaders with a good scientific and technical base. During the development of airless tires, new materials, technologies and designs can be created that will be used in the development and improvement of solutions that have real practical and commercial prospects [2].

## 2.1 Theoretical Studies of Airless Wheels

Since the start of implementation of airless wheels, the most common concept has been to use a layer of

elastomer with reinforced rings and a distinctive spoke pattern attached to the inside of the tire and distributed evenly around the rim. The set of spokes supports the weight of a vehicle and deforms to provide a shock-absorbing effect just like a pneumatic tire [7]. Therefore, research has been actively carried out on the stress-strain state of airless wheels in order to improve structural characteristics, for example, contact pressure [8] as well as the design of flexible spokes [9].

A significant contribution to the research and development of airless tires was made by scientists from Clemson University (USA), working together with Michelin, Oshkosh (military equipment) and others, as well as UNS Charlotte Academics (USA), Saint Louis University (USA). It should be noted that in the work of the employees of these institutions, the emphasis has primarily been made on the application of the finite element method.

Thus, in [10], the dynamic interaction of a Michelin Lunar Wheel with sandy soil and rock obstacles is modeled. The developed model makes it possible to estimate the deformations and local stresses of the structural elements of an airless tire, tire deflection and deformation of the supporting surface, longitudinal reactions and the nature of the distribution of normal pressure in the contact patch of the tire with the ground, vertical accelerations of the wheel hub when passing obstacles at different speeds.

The paper [11] examines three different non-pneumatic tire configurations from Michelin Tweel, Resilient Technologies and Bridgestone by searching for corresponding spoke designs. Quasi-static 2D analysis focuses on how spoke structures and shear layers influence tire contact pressure, vertical stiffness, and stresses. The results showed that the spoke shape has a great influence on the behavior of the tire in the second case, while the shear layer in the first case reduces the effect of the spoke shape change, especially in the contact pressure distribution.

The article [12] describes the process of creating a three-dimensional finite element model of a 195/50R16 radial tire and three types of airless tires with a spoke, honeycomb and lattice structure based on ABAQUS software, as well as the static and dynamic characteristics of the three finite elements tire models. The results show that in static analysis, the ground pressure of an airless tire is distributed on both sides of the tread. Stress concentration in tires mainly occurs in the surface area near the support spoke. The deformation zone of an airless tire mainly occurs in the contact area with the surface and near the contact spoke. When analyzing

the stable rolling state of a tire, the ground imprint of an airless tire is similar to that of a rectangular bar, and the ground pressure distribution is relatively uniform. The static and dynamic characteristics of a honeycomb airless tire are close to those of a tire with spokes. The article provides some reference materials on the structural design and optimization of airless tire parameters.

The article [13] presents an analytical model of an airless tire on hard ground without friction. The tire model consists of a thin flexible ring band and spokes that connect it to a rigid hub. The ring strip is modeled using curved beam theory, which takes into account deformations of bending, shear and tension around the circumference. The influence of the spokes, which are continuously distributed in the model and act as linear springs, is only taken into account under tension, resulting in a nonlinear response. An accurate parametric analysis of tire characteristics of interest is presented that can be used to support the optimal and rational design of appropriate non-pneumatic tires. The model was validated by comparison with two computational models using commercial software ABAQUS and experimental rolling resistance data.

Numerical modeling of the static and dynamic behavior of a non-pneumatic tire with various honeycomb spokes was carried out in [14]. In particular, the deformation modes, stress distribution and rolling resistance of a tire with honeycomb spokes were studied for the first time. The work is organized as follows: a simulation model is presented, including geometric size, material properties and numerical methods, and then the static properties of the model (deformation modes, stress distribution and load-carrying capacity) of tires designed with the same cell wall thickness as the honeycomb spokes. Deformation modes, stress distribution, and rolling resistance under dynamic loading are discussed.

Article [15] discusses methods for researching and designing non-pneumatic tires, and proposes a calculation model in the ANSYS environment.

Thus, reliable information about the stress-strain state of an airless wheel can be obtained only on the basis of the development of a methodology that combines the tools of both analytical and numerical research methods (finite elements method). The development of a method for calculating airless tires is an important step towards the possibility of technical implementation, creation and optimization of the design of airless tires.

## 2.2 Application of additive technologies in production of light personal electric vehicles and their components

One of the positive aspects of 3D printing usage is the ability to vary the properties of the resulting part by changing its internal structure in different sections (density, filling pattern and thickness of external contours).

Known attempts to manufacture experimental designs of electric motors, electric scooters, bicycles and motorcycles by additive technologies, being implemented even at the level of research work, arouse significant interest in the scientific community and industrial organizations.

Application of additive manufacturing for motorcycles is quickly developing. Thus, TE Connectivity presented the world's first motorcycle printed on a 3D printer and capable of moving at the exhibition Rapid 2015.

Metal 3D printing technologies (steel, titanium, aluminum) have found their application in the production of bicycles. In particular, a bicycle with a stainless steel frame was created in the Netherlands using a modern 3D printer. Additive technologies are widely used by manufacturers of bicycle components in many countries. A bicycle made entirely by 3D printing was presented in Belgium. The Solid titanium bicycle has been manufactured by the company Industry (Portland) in partnership with Ti Cycles on the base of additive technologies.

However, even taking into account all these facts, it is too early to say that such technologies can be applied without great efforts - these solutions are technologies of the 5-6 waves of innovation, requiring not only serious material investments, but also significant intellectual work.

Therefore, the development of production technologies as itself suggests the need to work in this extremely promising direction for science and production. The importance of carrying out research in this area is due to the high potential of additive technologies for manufacturing in the future [16].

It should be noted that currently there are various additive technologies (EBM, SLS, MJM, SLA and others) [17 - 21]. In this case, the choice of a specific technology is carried out as a result of a set of studies aimed at ensuring the performance characteristics of parts manufactured using 3D printing.

At the same time, additive technologies have some disadvantages, which include:

- insignificant dependence of the price of one product on the number of products in the production series;

- significant time consumption in the manufacture of a large number of products;
- loss of advantages in time compared to traditional technologies when using post-printing processing of products;
- limited list of raw materials used in printing;
- limitations on the strength and reliability of product characteristics;
- less accessibility of the method due to the higher complexity and cost of equipment and starting material;
- the roughness of the resulting surface of the product is within Ra 6.3 - 12.5 microns, which in some cases requires additional mechanical processing;
- lower strength of parts compared to cast analogues.

A conventional tire is a product of complex composites. It consists primarily of a reinforced toroid mounted on a metal rim. Since the advent of the newly invented non-pneumatic tires (airless wheels), the most common concept has been to use a layer of elastomer with reinforced rings and a distinctive spoke structure attached to the inside of the tire and evenly distributed around the rim. Currently, one of the most common solutions for airless wheels is to replace the air within the toroidal volume around the rim with discrete spokes distributed evenly between the inner and outer rings. In such structures, the spokes play the role of elastic elements that deform or bend in accordance with the magnitude of the load applied in the radial direction and, therefore, provide the necessary rigidity. For most existing solutions, the main challenges are limited ride quality (directly related to the number of spokes), limited fatigue resistance in stress areas, vulnerability to debris entrapment that can create imbalance, and the potential for increased noise due to spoke vibration and air circulation through open sidewalls surfaces.

As a rule casting is using in the manufacture of airless tires [13-16]. At the same time, the technical realization of airless tires and optimization of their shape can be further developed due to the spread implementation of additive technologies.

Therefore, the task of new airless wheel models development that will eliminate the dangers of conventional tires and be competitive with existing designs is urgent. At the same time, the additive technologies usage requires to carry out a complex of work not only in the development of the design of airless wheels, but also in terms of justifying the choice of materials and technologies used.

In this case, the development of a methodology that takes into account the mutual influence of not only

structural elements (shape, load), but also their technology is of particular importance.

### 3 Problem solution

#### 3.1 Calculation of the radial stiffness of elastic elements (spokes)

While having a number of advantages, pneumatic tires have significant disadvantages associated with the presence of air pressure inside it. The load-bearing capacity of airless tires is largely determined by the rigidity characteristics of the elastic elements and, above all, radial stiffness.

It is obvious that the implementation of internal damping is inextricably linked, first of all, with optimizing the shape of the spokes of an airless wheel: the arc-shaped spokes used or spokes that are an analogue of a honeycomb structure, being a decision of the problem, however, do not fully implement the existing capabilities for its solution.

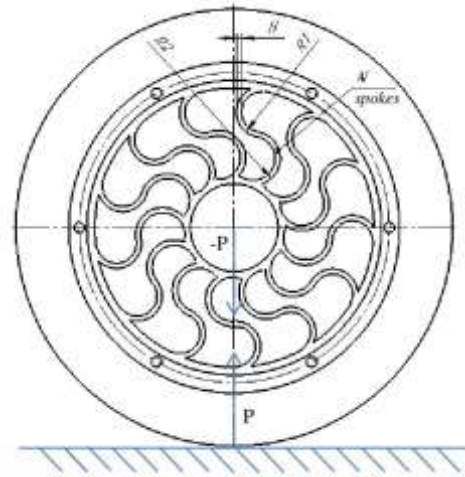
As an acceptable solution, the design of the spokes in the form of S-shaped twisted springs can be adopted (Fig. 1). This solution is formulated by the need to ensure lateral rigidity of the wheel with a minimum number of parts and components of the product. Usage of coil springs in such structures leads to the need for a guide vane in the final product. However, due to their shape, flat coil springs act as a lateral stiffener.

Let us introduce a hypothesis according to which elastic elements are considered as a continuous elastic medium. In this case, for any point on the rim, the force acting from the elastic element will be proportional to the radial displacement of the corresponding point on the rim  $\omega$ . Thus, for the  $i$ -th elastic element (Fig. 1), the force  $P_i$  will be related to the radial movement of the rim point  $\omega_i$  by the relations

$$P_i = C \cdot \omega_i, \quad i = \overline{1, N}, \quad (1)$$

where  $C$  is the radial stiffness of the elastic element, N/m.

Figure 1. Proposed design of an airless wheel and its loading scheme



To determine the radial stiffness of the elastic element, it is necessary to calculate the displacement of section A under the action of force  $P_i$  in the direction of this force. This displacement can be determined using Castigliano's theorem [22].

$$\omega_i = \frac{\partial U}{\partial P_i}, \quad (2)$$

where  $U$  is the potential energy of the elastic element.

For an elastic element, in which the main role is played by bending stresses, the displacements due to tension and shear are as small compared to the bending displacements as the energy of tension and shear compared to the bending energy.

Therefore, the formula for the potential energy of the bending of the element (taking into account the constant transverse section of the element along the length) will have the form

$$U = \frac{1}{2} \cdot \frac{\int M_{P_i}^2 dz}{EJ}, \quad (3)$$

where:  $dz$  - the length of the elementary section of the elastic element;

$M_{P_i}$  - function of the bending moment due to the action of force  $P_i$ ;

$E$  - modulus of elasticity of the elastic element;

$J$  - moment of inertia of the section;

$l$  - integration is carried out along the length of the beam.

The radial stiffness  $C_i$  of the elastic element is determined from expressions (1) – (3)

$$C_i = \frac{P_i}{\frac{\partial U}{\partial P_i}} = \frac{P_i}{\omega}, \quad (4)$$

where  $P_i$  is the effective radial force,  $\omega$  is the radial displacement of the corresponding point on the rim

The study of the stressed state of the elastic element and the rim of an airless tire under the action of a radial force (Fig. 1) can be carried out using the method described in [22].

If spokes are considered as a continuous elastic medium, then the force acting from the spokes for any point on the rim will be proportional to the radial displacement of the corresponding point of the rim  $\omega$  (in this case, obviously, the shape of the spokes - rectilinear or s-shaped - does not matter). Thus, this problem is an analogue of the problem of calculating a ring on an elastic base. There are  $N/2\pi R$  spokes per unit rim length. From the side of each spoke, the force  $EF\omega/l$  acts on the rim, where  $l$  is the length of the straight segment connecting the extreme points of the s-shaped spoke ( $l \sim R$ ),  $F$  is the cross-sectional area of a spoke.

Thus, the following force acts on a unit of rim

$$\frac{E \cdot F \cdot n}{2\pi R^2} \omega = k\omega,$$

wherefrom

$$k = \frac{E \cdot F \cdot n}{2\pi R^2} \quad (5)$$

Let's create a differential equation for the elastic line of the ring. As an independent variable we choose the angle  $\varphi$ , measured from the top of the ring (Fig. 2).

We select from the ring an elementary section of length  $R d\varphi$  and apply internal forces  $N$ ,  $Q$  and  $M$  in the sections produced. From the side of the spokes, a force  $k\omega R d\varphi$  will act on this section. Let's create equilibrium equations for this elementary section. If we project all forces onto the radial axis, then we get

$$\frac{dQ}{d\varphi} = N + kR\omega$$

The condition that the sum of the projections of all forces on an axis tangent to the arc of a circle is equal to zero gives

$$\frac{dN}{d\varphi} + Q = 0.$$

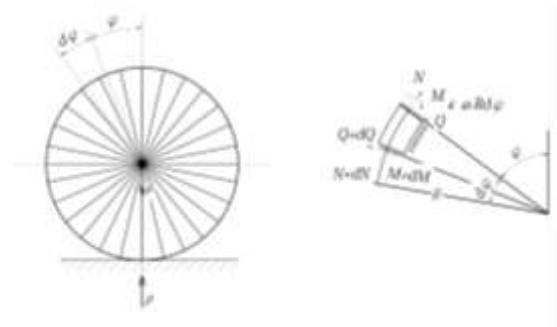
Let us equate to zero the sum of moments of forces relative to the point O

$$R \frac{dN}{d\varphi} + \frac{dM}{d\varphi} = 0$$

and exclude  $Q$  and  $N$  from these equations. Then we have

$$k \cdot R^2 \frac{d\omega}{d\varphi} = \frac{dM}{d\varphi} + \frac{d^3 M}{d\varphi^3}.$$

Figure 2. Determination of variable  $\varphi$



Deviation of the curvature  $\Delta (1/\rho)$  is connected with the bending moment  $M$  by the following relation

$$M = E \cdot J \cdot \Delta \left( \frac{1}{\rho} \right);$$

but, as it is known,

$$\Delta \left( \frac{1}{\rho} \right) = - \left( \frac{\omega}{R^2} + \frac{1}{R^2} \cdot \frac{d^2 \omega}{d\varphi^2} \right)$$

Since with positive displacement  $\omega$  directed from the center of the circle, the curvature of the ring decreases, there is a minus sign on the right side of this expression. The change in curvature in this expression consists of two quantities. The first term  $\omega/R^2$  corresponds to the change in curvature due to simple expansion of the ring. The second term

$$\frac{1}{R^2} \cdot \frac{d^2 \omega}{d\varphi^2},$$

equal to  $d^2\omega/ds^2$ , represents the usual change in curvature that is observed in a straight beam.

The differential equation after substituting  $M$  takes on the following final form:

$$\frac{d^5 \omega}{d\varphi^5} + 2 \frac{d^3 \omega}{d\varphi^3} + a^2 \frac{d\omega}{d\varphi} = 0,$$

where

$$a^2 = \frac{R^4 k}{EJ} + 1 \quad (6)$$

The solution to this equation can be written in the form

$$\omega = C_0 + C_1 \operatorname{ch} \alpha \varphi \cdot \cos \beta \varphi + C_2 \operatorname{sh} \alpha \varphi \cdot \sin \beta \varphi + C_3 \operatorname{ch} \alpha \varphi \cdot \sin \beta \varphi + C_4 \operatorname{sh} \alpha \varphi \cdot \cos \beta \varphi$$

where

$$\alpha = \sqrt{\frac{a-1}{2}}, \quad \beta = \sqrt{\frac{a+1}{2}}. \quad (7)$$

Since the ring is deformed symmetrically about the vertical axis, the function  $\omega$  must be even, i.e. when the sign of  $\varphi$  changes from plus to minus, it should remain unchanged. Therefore, we assume that arbitrary constants  $C_3$  and  $C_4$  appearing at odd functions are equal to zero.

The remaining constants are determined from the following conditions:

$$a) \varphi = \pi \Rightarrow \frac{d\omega}{d\varphi} = 0,$$

$$b) \varphi = \pi \Rightarrow Q = -\frac{P}{2},$$

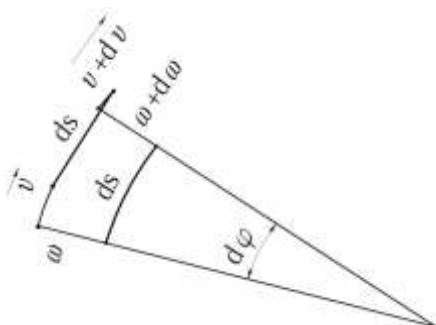
$$c) \int_0^{\pi} \omega d\varphi = 0.$$

The last condition means that when the wheel is loaded, the upper and lower points remain on the same vertical. Indeed, if we consider the element of the wheel rim before and after deformation (Fig. 3), it is easy to establish that the condition for its inextensibility will be written in the form

$$dv + \omega \cdot d\varphi = 0,$$

where  $v$  – movement along a tangent to the contour arc, or  $v = -\int \omega \cdot d\varphi$ .

Figure 3. Rim element before and after the deformation



Since there is no tangential displacement at the points  $\varphi=0$  and  $\varphi=\pi$ , this implies condition c).

When  $C_3=C_4=0$  the expressions for bending moment

$$M = -\frac{EJ}{R^2} \left( \omega + \frac{d^2\omega}{d\varphi^2} \right)$$

and shear force

$$Q = \frac{1}{R} \cdot \frac{dM}{d\varphi}$$

take the forms

$$M = -\frac{EJ}{R^2} (C_0 - 2\alpha \cdot \beta \cdot C_1 \cdot sh\alpha\varphi \cdot \sin \beta\varphi + 2\alpha \cdot \beta \cdot C_2 \cdot ch\alpha\varphi \cdot \cos \beta\varphi),$$

$$Q = 2\alpha \cdot \beta \cdot \frac{EJ}{R^3} [(\alpha \cdot C_1 + \beta \cdot C_2) \cdot ch\alpha\varphi \cdot \sin \beta\varphi + (\beta C_1 - \alpha C_2) \cdot sh\alpha\varphi \cdot \cos \beta\varphi]$$

Expanding the boundary conditions a), b) and c), we obtain

For a)

$$C_1[\alpha \cdot sh\alpha\pi \cdot \cos \beta\pi - \beta \cdot ch\alpha\pi] + C_2[\beta \cdot sh\alpha\pi \cdot \cos \beta\pi + \alpha \cdot ch\alpha\pi \cdot \sin \beta\pi] = 0,$$

For b)

$$C_1(\alpha \cdot ch\alpha\pi \cdot \sin \beta\pi + \beta \cdot sh\alpha\pi \cdot \cos \beta\pi) - C_2(\alpha \cdot sh\alpha\pi \cdot \cos \beta\pi - \beta \cdot ch\alpha\pi \cdot \sin \beta\pi) = -\frac{P}{4EJ} \cdot \frac{R^3}{\alpha\beta}$$

For c)

$$C_0\pi + \frac{C_1}{\alpha^2 + \beta^2} (\alpha \cdot sh\alpha\pi \cdot \cos \beta\pi + \beta \cdot ch\alpha\pi \cdot \sin \beta\pi) + \frac{C_2}{\alpha^2 + \beta^2} (\alpha \cdot ch\alpha\pi \cdot \sin \beta\pi - \beta \cdot sh\alpha\pi \cdot \cos \beta\pi) = 0.$$

Solving these equations, we get

$$C_0 = \frac{PR^3}{2\pi \cdot a^2 EJ},$$

$$C_1 = -\frac{P}{4EJ} \frac{R^3}{\alpha\beta} \frac{\alpha \cdot ch\alpha\pi \cdot \sin \beta\pi + \beta \cdot sh\alpha\pi \cdot \cos \beta\pi}{a(sh^2\alpha\pi + \sin^2 \beta\pi)},$$

$$C_2 = \frac{P}{4EJ} \frac{R^3}{\alpha\beta} \frac{\alpha sh\alpha\pi \cdot \cos \beta\pi - \beta ch\alpha\pi \cdot \sin \beta\pi}{a(sh^2\alpha\pi + \sin^2 \beta\pi)}.$$

Finally, the expressions for  $\omega$  and  $M$  take the forms:

$$\omega = \frac{P \cdot R^3}{4\alpha \cdot \beta \cdot E \cdot J} \left( \frac{2\alpha \cdot \beta}{\pi \cdot a^2} - A \cdot ch\alpha\varphi \cdot \cos \beta\varphi + B \cdot sh\alpha\varphi \cdot \sin \beta\varphi \right), \quad (8)$$

$$M = -\frac{PR}{2} \left( \frac{1}{\pi \cdot a^2} + A \cdot sh\alpha\varphi \cdot \sin \beta\varphi + B \cdot ch\alpha\varphi \cdot \cos \beta\varphi \right),$$

where

$$A = \frac{\alpha \cdot ch\alpha\pi \cdot \sin \beta\pi + \beta \cdot sh\alpha\pi \cdot \cos \beta\pi}{a(sh^2\alpha\pi + \sin^2 \beta\pi)}, \quad (9)$$

$$B = \frac{\alpha \cdot sh\alpha\pi \cdot \cos \beta\pi - \beta \cdot ch\alpha\pi \cdot \sin \beta\pi}{a(sh^2\alpha\pi + \sin^2 \beta\pi)}.$$

The force per one spoke will obviously be equal to

$$P_i = \frac{EF}{R} \omega \quad (10)$$

Expression (4) will then take the form

$$C = \frac{4\alpha \cdot \beta \cdot E \cdot J}{R^3 \left( \frac{2\alpha \cdot \beta}{\pi \cdot a^2} - A \cdot ch\alpha\varphi \cdot \cos \beta\varphi + B \cdot sh\alpha\varphi \cdot \sin \beta\varphi \right)} \quad (11)$$

From (10)-(11) it follows that

$$R = 2 \sqrt{\frac{\alpha \cdot \beta \cdot J}{F \left( \frac{2\alpha \cdot \beta}{\pi \cdot a^2} - A \cdot ch\alpha\varphi \cdot \cos \beta\varphi + B \cdot sh\alpha\varphi \cdot \sin \beta\varphi \right)}} \quad (12)$$

Taking into account the fact that the moment of inertia of a circular cross-section having a diameter  $d$  (diameter of the spokes) is determined by the formula

$$J = \frac{\pi \cdot d^4}{64},$$

and

$$F = \frac{\pi \cdot d^2}{4},$$

expression (12) takes the form

$$R = \frac{d}{2} \sqrt{\frac{\alpha \cdot \beta}{\frac{2\alpha \cdot \beta}{\pi \cdot a^2} - A \cdot ch\alpha\varphi \cdot \cos \beta\varphi + B \cdot sh\alpha\varphi \cdot \sin \beta\varphi}} \quad (13)$$

Taking into account (11) and (13), rigidity  $C$  can be represented as

$$C = \frac{\pi \cdot d \cdot E}{2} \sqrt{\frac{\frac{2\alpha \cdot \beta}{\pi \cdot a^2} - A \cdot ch\alpha\varphi \cdot \cos \beta\varphi + B \cdot sh\alpha\varphi \cdot \sin \beta\varphi}{\alpha \cdot \beta}}$$

where  $d$  is the diameter of the wheel spokes.

Thus, a methodology has been proposed for selecting the design parameters of an airless wheel for an electric personal mobility device, based on the use of analytical research methods, the results of which can be used as input data for the subsequent application of numerical methods (e.g. finite element method).

### 3.2 Calculation of the radial stiffness of elastic elements (spokes)

Usage of equations (14) opens up opportunities for increasing the accuracy of calculations of airless wheels. Thus, by specifying different values of the parameters of an airless wheel, it seems possible to establish their influence on the distribution of external loads.

All this indicates the advisability of using a multilateral assessment of calculated values. Let's look at the proposed solutions using the Xiaomi Mijia M 365 electric light scooter as an example.

From expressions (5) and (6), assuming the elastic modulae of the spokes and rim to be equal, we obtain:

$$\alpha^2 = \frac{R^2 F n}{2\pi J} + 1 = \frac{\pi \cdot 0.2^2}{4} \cdot 36 \cdot 31^2 + 1 = 577.7 \Rightarrow \alpha = 24.04,$$

According to (7), we can calculate

$$\alpha = \sqrt{\frac{24,04 - 1}{2}} = 3,395,$$

$$\beta = \sqrt{\frac{24,04 + 1}{2}} = 3,539.$$

Now it can be found, that

$$sh \alpha\pi \approx ch \alpha\pi \approx \frac{1}{2} e^{10,66},$$

$$\sin \beta\pi = -0,992, \quad \cos \beta\pi = 0,1223.$$

According to (9) we have:

$$A = -0,245e^{-10,66}, \quad B = 0,326e^{-10,66}.$$

Formulae (8) and (10) can be rewritten in the forms:

$$M = P(-0,00855 + 3,80e^{-10,66}sh \alpha\varphi \cdot \sin \beta\varphi - 5,05e^{-10,66}ch \alpha\varphi \cdot \cos \beta\varphi)$$

$$P_c = P(0,0278 + 0,514e^{-10,66}ch \alpha\varphi \cdot \cos \beta\varphi + 0,683e^{-10,66}sh \alpha\varphi \cdot \sin \beta\varphi).$$

It follows that for small values of  $\varphi$  the second and third terms in brackets will be very small and will not significantly affect the values of  $M$  and  $P_c$ . Based on the last dependencies, it is possible to construct diagrams of the bending moment  $M$  and forces on the spokes  $P_c$  (Fig. 4).

It is not difficult to establish that for a driver weighing 77 kg and a scooter weighing 3 kg, a force of 40 kg is exerted on the rear wheel. Then we find that  $M_{max} = 88$  kN, and the greatest force on the spoke  $P_{c max} = 11.2$  kg.

Obviously, the result obtained does not take into account the pre-tension of the spokes, which is forming during assembly, but it should not exceed  $P_{c max}$  in absolute value.

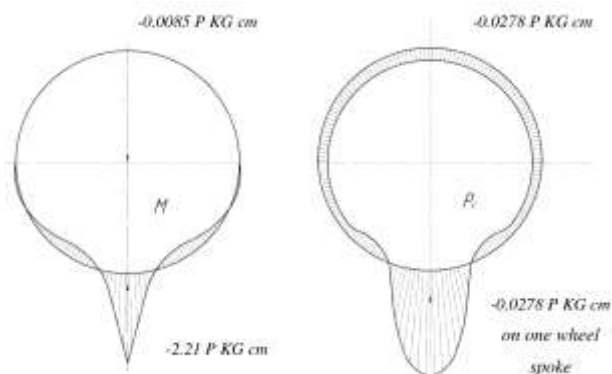
It follows from (10) that

$$P_{i max} = \frac{EF}{R} \omega_{max},$$

so taking into account the above calculations

$$\omega_{max} = 11.2 \cdot \frac{R}{EF}.$$

Figure 4. Diagrams of the bending moment  $M$  and forces on the spokes  $P_c$



The Xiaomi Mijia M 365 light scooter does not have shock absorbers, so if we consider the wheel radius  $R$  as a function of two variables ( $R(E, F)$ ), where  $E$  is the elastic modulus, which takes into account not only the properties of the material, but also the printing technology used and  $F$  is the area cross section of the spokes, then it will not have extrema (first-order partial derivatives will be different from

0). At the same time, we can consider the problem of finding local extremes that exist in the permissible range of changes in  $E$  and  $F$ .

It follows from (14) and the above calculations of the coefficients that the function where  $C_{wheel} = 150$  N/mm can be chosen as the objective function.

A numerical calculation was performed, and it was found that at  $E = 2140$  MPa and  $H = 2.2$  mm, a solution to the optimization problem was achieved.

In order to check the results of the model calculation, the design research module of the Solidworks software package was used. As a result of the research, a calculation model was created with fixed landing dimensions and free dimensions of the geometry of the damper spokes (Fig. 5-6). Static and working loads were specified, and an analysis of the deformed state of the rim spokes was performed in the Simulation environment. The thicknesses of the spokes were defined as the variable parameters used. The radii  $R_1$  and  $R_2$  are dependent on the thickness of the spoke  $H$  and are adjusted automatically. A total of 43 possible scenarios were analyzed with optimization parameters - stresses at all points of the part are less than the yield strength at a minimum mass of the part. The number of scenarios and analysis time are directly related to the computing capabilities of the PC. The maximum deformation under the applied loads was 4.0 mm without destruction (Fig. 7).

Figure 5. Finite element model of the airless wheel for Xiaomi Mijia M 365 light scooter

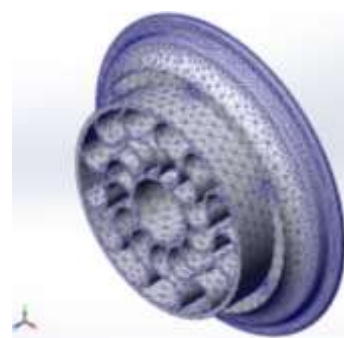


Figure 6. Stress diagram of rim spokes

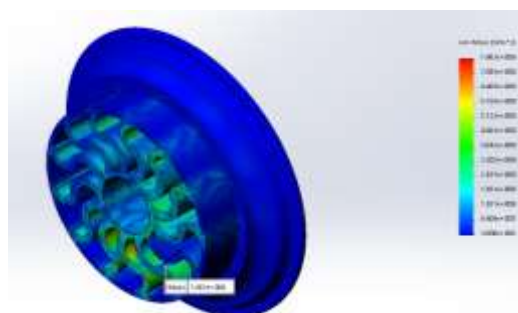
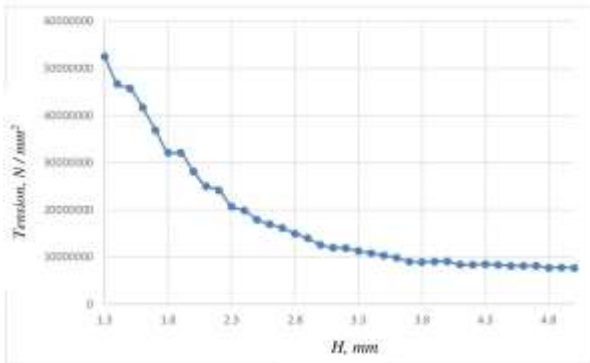


Figure 7. Dependence of changes in maximum stresses on the thickness of the spoke H



### 3.3 Study of the influence of filling parameters of samples manufactured using 3-D printing on their fatigue resistance

FDM technology (one of the most commonly used additive processes) is typically used to print details of complex geometries, necessary in the medical, aerospace and automotive industries. Most research in the development of FDM technologies has focused on obtaining the geometric accuracy of the parts, but relatively little research has been done on the mechanical properties of the final products. At the same time, this method makes it possible to obtain a huge variety of structures and filling densities of parts, and, therefore, provides the user with an effective tool for creating prototypes with given design and technological parameters.

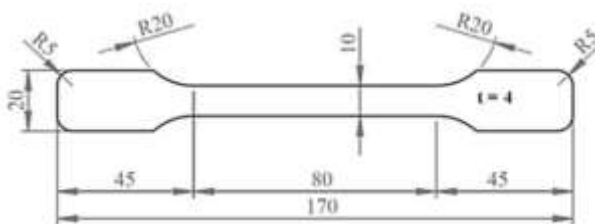
Therefore, the purpose of this study is to investigate the influence of filling density on the mechanical properties of the samples in order to optimize time and material costs in the production of details.

PLA plastic was used as the printing material.

A TEVO Michelangelo 3D printer was used to print the samples. Its technological parameters are the following: nozzle diameter 0.4 mm, printing speed 60 mm/s, print head temperature – 220°C, 2 outer layers of solid filling.

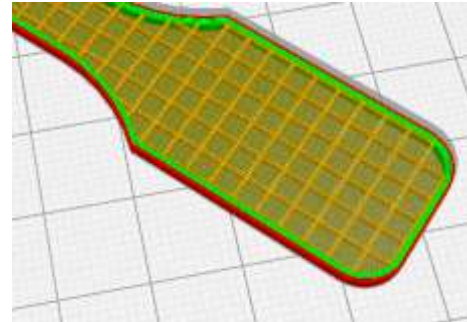
A type 1A sample according to ISO 527-2:2012 was used for testing (Fig. 8).

Figure 8. Sample of type 1A according to ISO 527-2:2012



A rectilinear part filling scheme was chosen when printing. Samples were made in 5 pieces in increments of 10%, starting from 10% until the internal volume of the part was completely filled (Fig. 9).

Figure 9. Sample filling scheme



The characteristics of the plastic used in the manufacture of samples are given in Table 1, and the printing parameters are shown in Table 2. To select the filling pattern of the part, a series of tensile and compression tests were carried out on the samples. When carrying out tensile tests, a sample of type 1A according to ISO 527-2:2012 was used, and for compression tests, a cube with a side of 15 mm was used.

Table 1. Characteristics of plastic used in 3-D printing

Characteristics	Value
Melting temperature	173-178°C
Softening point	50°C
Hardness (Rockwell)	R70-R90
Elongation at break	3.8%
Flexural strength	55.3 MPa
Tensile strength	57.8 MPa
Tensile modulus	3.3 GPa
Flexural modulus	2.3 GPa
Glass transition temperature	60-65°C
Density	1.23-1.25 g/cm³
Minimum wall thickness	1.0 mm
Printing accuracy	± 0.1%
The size of the smallest parts	0.3 mm
Shrinkage during product manufacturing	no
Moisture absorption	0.5-50%

Table 2. Sample Printing Options

Parameters	Value
Nozzle temperature	200(±2)°C
Table temperature	50(±3)°C
Layer thickness	0.28 mm
Wall thickness	0.8 mm
Bottom/lid thickness	0.84 mm
Filling Density	30%
Print speed	75 mm/s
Plastic	PLA (China)
Printer	Ortur V4

The results of tensile-compression tests of samples are shown in Table 3, and comparative data from the tests performed are shown in Fig. 10 – 11.

As a result of the tests, it was found in particular, that sample No. 6 with a filling density of 60% has optimal tensile strength (Fig. 10).

Figure 10. Comparison of tensile test results for samples

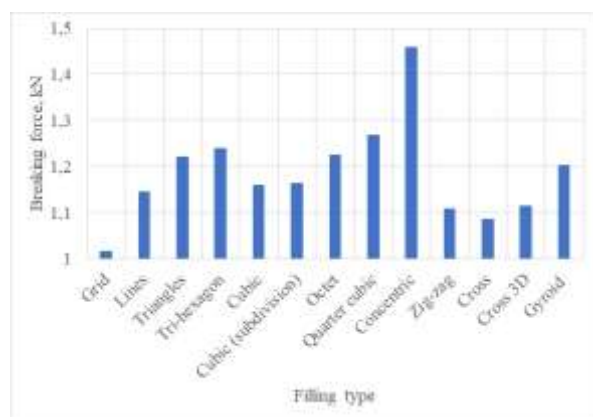
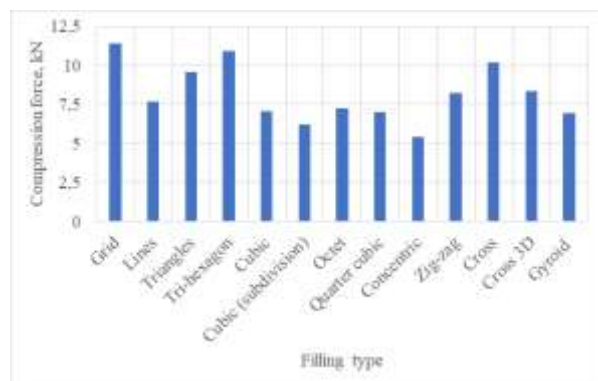


Figure 11. Comparison of compression test results for samples



It should be noted that the proposed solution method provides a number of possibilities both from the point of view of taking into account different options for the design of wheel spokes (taking into account different radii), and from the point of view of the possibilities offered by additive technologies (taking into account different values of Young's moduli for the design under consideration, reflecting the nature of the filling of the element when 3D printing).

Table 3. Results of testing samples for tension and compression

N	View of pattern filling	Tensile strength, kN	Compressive strength, kN
1		1.017	11.38
2		1.146	7.66
3		1.222	9.57
4		1.239	10.94
5		1.161	7.06
6		1.165	6.22
7		1.226	7.25
8		1.269	7.03
9		1.459	5.40
10		1.109	8.22
11		1.087	10.17
12		1.115	8.37
13		1.203	6.97

Table 3. Test results for samples of different filling densities

N	Filling density, %	Average stress value, MPa
1	10	25.37
2	20	25.48
3	30	25.73
4	40	33.28
5	50	35.88
6	60	49.83
7	70	52.35
8	80	55.80
9	90	62.17
10	100	71.70

### 3.3 Findings/Results

The solutions obtained can be used in the manufacture of an airless wheel with internal damping, in particular, using the extrusion method. As it can be seen from the simulation results, the rim spokes are under predominantly tensile loads. Based on the data obtained, we can conclude that for this part of the detail it is necessary to use a concentric filling pattern. To correlate the data with the simulation results, 100% part filling was chosen. The wheel rim is under the complex deformations from compression-tension during operation of alternating loading. In accordance with the test results, to reduce unsprung masses (Table 4), the outer rim was made with an incomplete filling of 30%, the filling pattern is a hexagon formed by triangles (this type of filling showed high, relative to other samples, strength indicators both in tensile tests and compression tests) (Fig. 10-11).

Figure 12. Tensile testing of samples

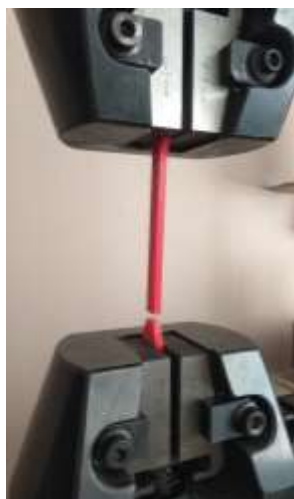


Figure 13. Internal structure of the wheel rim (internal rim filling (30%, hexagon pattern formed by triangles)



Figure 14. Airless wheel assembly installed on the Xiaomi Mijia M365 electric light scooter



Figure 15. General view of the test setup



The coefficient  $C_z$  of tire's normal stiffness is the first derivative of the normal wheel load  $P_z$  with respect to the normal tire deflection  $h_z$ :

$$C_z = \frac{\partial P_z}{\partial h_z}, \quad (15)$$

where normal tire deflection  $h_z$  is the linear displacement of the wheel center relative to the supporting surface under the influence of normal

load, measured by the normal to the supporting surface.

Figure 16. Imprint of a standard (left) and an airless wheel (right), made using additive technologies

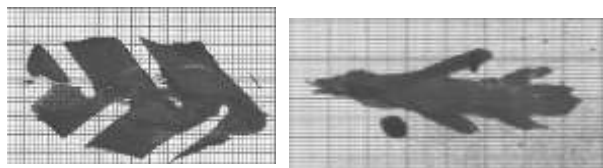
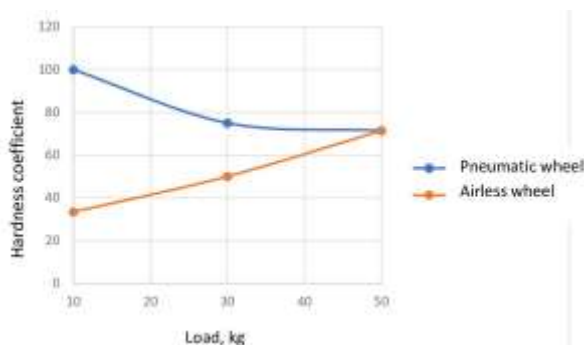


Table 4. Results of static tests

Sample	Contact patch area under load (mm <sup>2</sup> )			Contact patch area, load/lateral displacement 5 mm (mm <sup>2</sup> )		
	10 kg	30 kg	50 kg	10 kg	30 kg	50 kg
Pneumatic tire	676	1354	1711	811	1705	1760
Linear displacement of the wheel center, mm	1	4	7			
Airless wheel	510	760	940	914	1002	1256
Linear displacement of the wheel center, mm	3	6	7			

Figure 17. Dependence of normal stiffness coefficient of the load



Thus, the developed wheel has lower rolling resistance in the operating load range compared to a standard pneumatic tire. This is connected with the greater rigidity of the rubber bandage compared to a pneumatic tire as well as with the fact that the displacement of the wheel center occurs due to the deformation of the damper spokes, and not the tire, which increases the contact area of the wheel and, as a result, the friction force on the road surface.

## 4 Conclusion

A technique has been developed that makes it possible to set optimal construction and technological parameters for the spokes of an airless wheel with internal damping during the transition to design synthesis, which is advisable to perform using the finite element method.

A methodology has been developed for designing damping elements of wheels based on a calculation model with optimization criteria in the form of maximum permissible movements of separate elements, the tensile strength of the material, taking into account the influence of rim geometry (rounding radii, thickness and number of spokes).

The density and shape parameters of the filling of separate wheel elements have been optimized. It has been shown that the maximum combination of tensile strength is achieved with a concentric filling pattern. The tests carried out showed the best economic indicators of the developed design. Further development of the design is possible through the usage of more complex geometry of spoke dampers to increase lateral stability during curvilinear movement of the electric light scooter, as well as the usage of composite plastics to reduce material consumption.

At the same time, the area of research related to the development of an intelligent system for detecting 3-D printing defects in the manufacture of critical parts of electrical light personal mobility means may be of particular interest. It should be noted that early detection of defects can make 3-D printing more popular, reliable and attractive. Currently, work is underway to develop software for image processing, making it possible to evaluate the progress of the printing process, to detect faults and defects, thus controlling the quality of 3-D printing. Work is underway to create an appropriate statistical database of printed samples.

### References:

- [1] A. Volochko, A., Yankevich, S., Yankevich, N. 3D printing application in personal light electric transport production in Belarus. *Proceedings of 8th Transport Research Arena TRA 2020*, April 27-30, 2020, Helsinki, Finland. –DOI: 10.13140/RG.2.2.26055.85924.
- [2] Yankevich, N., Yankevich, S. Robotization as one of the prospects for electromobility in Belarus. *International Journal of Robotics and Automation Technology*, 2019, vol. 6, pp. 24-42, DOI= <https://doi.org/10.31875/2409-694.2019.06.3>.

- [3] Gajewski V.J., 1992. Pat. US5223599A, Int. Cl. C08G 18/00. Polyurethane elastomer and non-pneumatic tire fabricated therefrom. Uniroyal Chemical Company, Inc. – № 866636; filed 10.04.1992; publ. date 29.06.1993.
- [4] Rhyne T.B., Thompson R.H., Cron S.M., Demino K.W., 2004. Pat. US7201194B2, Int. Cl. B60C 9/26. Non-pneumatic tire. Michelin Recherche et Technique S. A. – № 10/782999; filed 20.02.2004; publ. date 10.04.2007.
- [5] Gass, D.B., Bennett, J.D., Brady, L.J., Borud, E.J., Koenig, D.J., Peppel, K.W., 2017. Pat. US9573422B2, Int. Cl. B60C 7/12, B60B 9/00. Non-pneumatic tire. Polaris Industries Inc. – № 13/802474.
- [6] Choi, S.J., Kim, H.J., Kim, M.S., Ko, K.J., Kang, K.H., 2016. Pat. US9333799B2, Int. Cl. B60C 7/16, B60B 9/26, B60C 7/18. Non-pneumatic tire with reinforcing member having plate wire structure. Hankook Tire Co., Ltd. – № 13/954272.
- [7] Kim, K. and Kim, D. Contact Pressure of Non-Pneumatic Tires with Hexagonal Lattice Spokes. *SAE Technical Paper*, 2011, 2011-01-0099. DOI= <https://doi.org/10.4271/2011-01-0099>.
- [8] Summers, JD, Ziegert, J, Fadel, G. Compliant Hexagonal Meso-Structures Having Both High Shear Strength and High Shear Strain. *Proceedings of the ASME 2010 International Design Engineering Technical Conferences and Computers and Information in Engineering Conference*. Volume 2: 34th Annual Mechanisms and Robotics Conference, Parts A and B. Montreal, Quebec, Canada. August 15–18, 2010. pp. 533-541. ASME. DOI = <https://doi.org/10.1115/DETC2010-28672>.
- [9] Veeramurthy, M., Ju, J., Thompson, LL, & Summers, JD. Optimization of a Non-Pneumatic Tire for Reduced Rolling Resistance. *Proceedings of the ASME 2011 International Design Engineering Technical Conferences and Computers and Information in Engineering Conference*. Vol. 8: 11th International Power Transmission and Gearing Conference; 13th International Conference on Advanced Vehicle and Tire Technologies. Washington, DC, USA. August 28–31, 2011. pp. 861-868. ASME. DOI= <https://doi.org/10.1115/DETC2011-48730>.
- [10] Aboul-Yazid, A.M., Emam, M.A.A., Shaaban, S. and El-Nashar, M.A. Effect of spokes structures on characteristics performance of non-pneumatic tires. *International Journal of Automotive and Mechanical Engineering (IJAME)*, 2015, DOI= 10.15282/ijame.11.2015.4.0185.
- [11] Zhang, Z., Fu, H., Liang, X., Chen, X., Tan, D. Comparative Analysis of Static and Dynamic Performance of Nonpneumatic Tire with Flexible Spoke Structure. *Shandong University of Technology, School of Transportation and Vehicle Engineering, Chin*, 2020, DOI=10.5545/sv-jme.2020.6676.
- [12] Gasmi, A., Josepha, P.F., Rhyne, T.B., Cron, S.M., 2012. Development of a two-dimensional model of a compliant non-pneumatic tire. *International Journal of Solids and Structures*. DOI=10.1016/j.ijsolstr.2012.03.007.
- [13] Kim, K., Ju, J., Kim, S., Kim, D-M. Contact pressure of a non-pneumatic tire with three-dimensional cellularspokes. *Proceedings of the ASME 2011 International Mechanical Engineering Conference & Exposition IMECE*, 2011 DOI=10.1115/IMECE2011-64233.
- [14] Jin, X., Hou, C., Fan, X., Sun, Y., Lv, J., Lu, C. Investigation on the static and dynamic behaviors of non-pneumatic tires with honeycomb spokes. *Composite Structures*, 2017, DOI=10.1016/j.compstruct.2017.12.044.
- [15] Tychina, K.A. Development of a numerical methodology for calculating and designing metal-elastic wheels: dissertation. *Ph.D. tech. Sciences*: 01.02.2006. Moscow State Tech. University named after N.E. Bauman, 2001, 120 p.
- [16] Yankevich, S.N. Nanostructured materials and additive technologies for personal electric transport. *Science and Innovation* (2021), No. 1, P. 34-41. DOI = <https://doi.org/10.29235/1818-9857-2021-1-34-41>
- [17] Litunov, S.N., Slobodenyuk, V.S., Melnikov, D.V. Review and analysis of additive technologies. Part 1. *Omsk Scientific Bulletin*. No. 1, 2016, P. 12 – 17.
- [18] Monfared, M., Ramakrishna, S., Nasajpour-Esfahani N., Toghraie, D., Hekmatifar M., Rahmati, S. *Science and Technology of Additive Manufacturing Progress: Processes, Materials, and Applications*. - *Metals and Materials International* (2023) 29:3442–3470, DOI= <https://doi.org/10.1007/s12540-023-01467-x>.
- [19] Niu, X., Zhu, S., He, J., Liao, D., Correia, J.A.F.O., Berto, F., Wang, Q. Defect tolerant fatigue assessment of AM materials: size effect

- and probabilistic prospects. *Int. J. Fatigue* 160, 106884 (2022). DOI=<https://doi.org/10.1016/j.ijfatigue.2022.106884>
- [20] Ren, W., Mazumder, J., In-situ porosity recognition for laser additive manufacturing of 7075-Al alloy using plasma emission spectroscopy. *Sci. Rep.* 10, 19493 (2020). DOI=<https://doi.org/10.1038/s41598-020-75131-4>.
- [21] Ghanem, M.A., Basu, A., Behrou, R., Boechler, N., Boydston, A.J., Craig, S.L., Lin, Y., Lynde, B.E., Nelson, A., Shen, H., Storti, D.W. The role of polymer mechanochemistry in responsive materials and additive manufacturing. *Nat. Rev. Mater.* 6, 84–98 (2021). DOI=<https://doi.org/10.1038/s41578-020-00249-w>.
- [22] Feodosiev, V.I. Strength of materials. M.: Publishing house of MSTU im. N.E. Bauman, 1999, 592 p.

### **Contribution of Individual Authors to the Creation of a Scientific Article (Ghostwriting Policy)**

The authors equally contributed in the present research, at all stages from the formulation of the problem to the final findings and solution.

### **Sources of Funding for Research Presented in a Scientific Article or Scientific Article Itself**

No funding was received for conducting this study.

### **Conflict of Interest**

The authors have no conflicts of interest to declare that are relevant to the content of this article.

### **Creative Commons Attribution License 4.0 (Attribution 4.0 International, CC BY 4.0)**

This article is published under the terms of the Creative Commons Attribution License 4.0

[https://creativecommons.org/licenses/by/4.0/deed.en\\_US](https://creativecommons.org/licenses/by/4.0/deed.en_US)